Interpretation of measurements of the global momentum and energy confinement times in strongly rotating tokamak plasmas

1991 Nucl. Fusion 31 31

(http://iopscience.iop.org/0029-5515/31/1/004)

INTERPRETATION OF MEASUREMENTS OF THE GLOBAL MOMENTUM AND ENERGY CONFINEMENT TIMES IN STRONGLY ROTATING TOKAMAK PLASMAS

W.M. STACEY, Jr.
Fusion Research Center,
Georgia Institute of Technology,
Atlanta, Georgia,
United States of America

ABSTRACT. A model is presented for the self-consistent interpretation of the global momentum and energy confinement times and the central rotation velocities measured in plasmas that are rotating at speeds comparable to their thermal speed. This model incorporates corrections for non-steady state and represents the effect of radial density, temperature and velocity profiles. The momentum transport model is based upon gyroviscosity theory, which remains controversial. Good agreement between measured and predicted rotation frequencies and momentum confinement times is obtained for a collection of JET data and for one TFTR beam power scan. The energy confinement is shown to be degraded by a viscous energy flux, which is predicted to account for up to one fourth of the total energy loss for the JET data and for one half of the energy confinement degradation measured in the TFTR beam power scan. This implies that the measured energy confinement times in strongly rotating plasmas are significantly shorter than the times of energy confinement against conductive and convective transport processes.

1. INTRODUCTION

When unbalanced neutral beam injection (NBI) is used to heat a tokamak plasma, the resulting torque causes the plasma to rotate. Rotation speeds comparable to the thermal speeds of impurity ions present in the plasma and well within a factor of ten of the thermal speed of the main plasma ion species are routinely achieved (see, for example, Refs [1–7]). In rotating plasmas there are new transport effects associated with the viscous radial transfer of momentum and with the plasma inertia which are not found in non-rotating plasmas. In some instances, the plasma does not reach a rotational equilibrium. These viscous, inertial and acceleration effects must be taken into account in interpreting measurements made for the purpose of obtaining information about global or local transport processes in a strongly rotating ($v_\phi \sim v_{th}$) plasma.

The purpose of this paper is to present a self-consistent formalism for interpreting measurements of rotation speeds, momentum confinement times and energy confinement times in a strongly rotating tokamak plasma and to apply this formalism to interpret measurements made in JET as an illustrative example. Self-consistency between experimental and theoretical definitions is achieved by using the appropriate, time dependent angular momentum and energy balance equations. The formalism is specifically designed to incorporate newly available measurements of velocity and temperature radial profiles. An essential element of the formalism is a model for the viscous radial transport of the angular momentum input by the unbalanced NBI from the centre to the edge of the plasma, where it is subsequently transferred to the wall or coil system by charge exchange, ripple viscosity, etc. The momentum transport model used in this paper is based on gyroviscosity [8]. There remains a controversy about the gyroviscous theory, which is discussed in Section 7.

The paper is organized as follows. In Section 2, a theory for the interpretation of central rotation velocity and momentum confinement measurements is presented, and approximations are introduced to reduce it to a computationally tractable form. In Section 3, the theory for rotational corrections to energy confinement time measurements is presented and reduced to a computational form. In Section 4, the formalism developed in Sections 2 and 3 is applied to analyse a number of recent JET pulses for which rotation frequency measurements were made. In Section 5, the formalism is applied to analyse a beam power scan in TFTR which is particularly well suited for analysis. A brief discussion of related work is given in Section 6. Finally, a summary and conclusions are presented in Section 7.

2. ROTATION VELOCITY AND ANGULAR MOMENTUM CONFINEMENT

2.1. Flux surface co-ordinate system

We use a right hand (ψ, p, ϕ) flux surface co-ordinate system (e.g. [9]) with differential length elements, $d\ell_x = h_x\,dx$, and a differential volume element,

$$V'(\psi) = 2\pi \oint_\psi \frac{d\ell_p}{B_p} \tag{1}$$

where B_p is the 'poloidal' magnetic field. The flux surface average of a quantity A is

$$\langle A \rangle \equiv 2\pi \oint_\psi \frac{A\,d\ell_p}{B_p} \Big/ V'(\psi) \tag{2}$$

in this co-ordinate system, and the volume integral of a quantity A is

$$\int_{\psi_0}^{\psi_a} \langle A \rangle\, V'(\psi)\,d\psi \tag{3}$$

where ψ_0 and ψ_a are the central and outermost flux surfaces, respectively.

2.2. Toroidal angular momentum balance

The toroidal angular momentum balance on the entire plasma is

$$\dot{L}_\phi + \pi_\phi = \Gamma_\phi \tag{4}$$

where

$$L_\phi \equiv \int_{\psi_0}^{\psi_a} \langle Rnmv_\phi \rangle V'(\psi)\,d\psi \tag{5}$$

is the angular momentum, R is the major radius, n is the particle density, m is the mass, v_ϕ is the rotation velocity,

$$\Gamma_\phi \equiv \int_{\psi_0}^{\psi_a} \langle R^2 \nabla\phi \cdot \vec{M}_b \rangle V'(\psi)\,d\psi \tag{6}$$

is the rate at which a torque is applied to the plasma by NBI, with $\vec{M}_b$ being the rate at which momentum is transferred from beam particles to plasma particles, and

$$\pi_\phi \equiv \int_{\psi_0}^{\psi_a} \langle R^2 \nabla\phi \cdot \nabla \cdot \vec{\vec{\pi}} \rangle V'(\psi)\,d\psi \tag{7}$$

is the rate at which angular momentum is transferred 'radially' out of the plasma by viscous processes, represented by the viscosity tensor $\vec{\vec{\pi}}$. At this point, the viscosity tensor is general and can represent neoclassical and 'anomalous' momentum fluxes. Momentum convection is estimated to be small and is neglected.

A sum over all species in the plasma is implied in these equations.

2.3. Experimental momentum confinement time

The actual definition of the quantity is not so important as is the self-consistency between the experimental and theoretical definitions. A definition, favoured by experimentalists [10, 11], in terms of the angular momentum replacement rate will be used:

$$\tau_\phi^{ex} \equiv \frac{L_\phi}{\Gamma_\phi - \dot{L}_\phi} = \frac{\hat{\tau}_\phi^{ex}}{1 - \beta\hat{\tau}_\phi^{ex}} \tag{8}$$

where

$$\hat{\tau}_\phi^{ex} \equiv L_\phi/\Gamma_\phi \tag{9}$$

$$\beta \equiv \dot{L}_\phi/L_\phi \tag{10}$$

are constructed from measured values of n and v_ϕ and from the calculated input torque.

2.4. Theoretical momentum confinement time

The theoretical quantity that is appropriate to be compared with Eq. (8) is found by using Eq. (4) to replace $\Gamma_\phi - \dot{L}_\phi$ by π_ϕ:

$$\tau_\phi^{th} \equiv L_\phi/\pi_\phi \tag{11}$$

Measured values of n, v_ϕ and whatever additional parameters that are involved in π_ϕ should be used to evaluate Eq. (11).

2.5. Theoretical central rotation velocity

Anticipating that $\pi = \pi(v_\phi)$, writing $v_\phi(\psi) = v(\psi_0)h_v(\psi) \equiv v_{\phi 0}h_v(\psi)$, and using Eq. (4) yields

$$\Omega_{\phi 0}^{th} \equiv \frac{v_{\phi 0}}{R_0} = \frac{(\Gamma_\phi/R_0)}{(\pi_\phi/v_{\phi 0}) + \frac{\partial}{\partial t}(L_\phi)/v_{\phi 0}} \tag{12}$$

Measured values of n, h_v and other parameters involved in π should be used to evaluate Eq. (12). Note that, since π_ϕ and $L_\phi \sim v_\phi$, the denominator in Eq. (12) is independent of $v_{\phi 0}$ (but depends upon $\dot{v}_\phi/v_{\phi 0}$).

2.6. Viscosity model

The above formalism is independent of the model for viscosity; however, its application requires specification of such a model. In all likelihood, several mechanisms — classical and anomalous — are involved in the radial transfer of toroidal momentum from the centre of the plasma to the external system. Here, a model is postulated in which the angular momentum is transferred from the centre to the edge of the plasma by gyroviscosity [8] and is then transferred by charge exchange, ripple viscosity or some other mechanism from the edge of the plasma to the external system. If the rate of momentum transfer from the plasma edge to the external system is fast compared to the rate of gyroviscous transfer from the centre to the edge of the plasma, which is postulated, then the gyroviscous transfer will determine the overall rate of momentum transfer experienced by the plasma and the model used herein is appropriate. The success of the gyroviscous model in explaining the rotation velocities measured in ISX-B, PLT and PDX [12], and the rough agreement between theory and experiment in preliminary analyses of D-III [4], TFTR [5, 6] and JET [7] encourage its adoption.

The rate of gyroviscous angular momentum transfer is given [8] by

$$\left\langle R^2 \nabla\phi \cdot \nabla \cdot \vec{\vec{\pi}}_j \right\rangle = -\left\langle \frac{1}{R h_p} \frac{\partial}{\partial \ell_\psi} \left(R^3 h_p \eta_4^j \frac{\partial \Omega_\phi^j}{\partial \ell_p} \right) \right\rangle \quad (13)$$

where

$$\eta_4^j = \frac{n_j m_j T_j}{Z_j e B} \quad (14)$$

for each species j.

The magnitude of the gyroviscous angular momentum transfer rate is proportional to the 'poloidal' variation in the rotation frequency, Ω_ϕ^j, over the flux surface. This variation is predicted [13, 14] to be $O(\epsilon)$ for impurities with $v_\phi^j = v_{th}^j$, but to be $\ll O(\epsilon)$ for the main plasma ions with $v_\phi^j \ll v_{th}^j$. Thus, the gyroviscous momentum transfer is primarily due to impurities.

It is possible that other phenomena could transfer momentum from the centre of the plasma to the edge, or directly to the external system, at a rate comparable to or faster than gyroviscosity. In this case, the other phenomena would substantially affect, or even dominate, the momentum transport. This is apparently the case for the 'locked modes' that are sometimes observed in JET [7], in which the rotation of the $n = 1$ mode and the bulk rotation of the plasma are both observed to vanish even though NBI continues. It is also possible that the momentum transfer from the plasma edge to the external system could be slower than that from the centre to the edge, in which case it would determine the overall momentum transfer rate. These possibilities could be included in the formalism by incorporating appropriate models in the evaluation of π_ϕ from Eq. (7).

2.7. Effective impurity model

It is impractical to evaluate Eq. (13) for each charge state of each ion species in the plasma. Information on concentrations is unlikely to be available. Even if it were, accurate models for calculating $\partial\Omega_\phi^j/\partial\ell_p$ are not available. For this reason, an effective impurity model will be used, and the product of normalized poloidal, $\tilde{\theta}$, and radial, G, profiles factors [8] will be set equal to unity. $\tilde{\theta} = 1$ is equivalent to setting $|\partial\Omega_\phi^j/\partial\theta| = \epsilon|\Omega_\phi^j|$.

In previous applications [12], the plasma ions were treated as a single effective species with charge state Z_{eff}.

Another model is introduced here for plasmas in which a single impurity species is predominant. In this case, charge neutrality, $n_e = n_i + Zn_z$, and the definition of Z_{eff}, $n_e Z_{eff} = n_i + Z^2 n_z$, yield

$$\frac{n_z}{n_e} = \frac{Z_{eff} - 1}{Z(Z-1)} \equiv \frac{1}{\bar{Z}}$$
$$\frac{n_i}{n_e} = \frac{Z - Z_{eff}}{Z - 1} \quad (15)$$

For the light to intermediate elements,

$$\frac{m_z}{Z} \simeq 2m_H = m_D \quad (16)$$

is a good approximation.

Using Eqs (15) and (16), the viscosity coefficient of Eq. (14) for the impurity species becomes

$$\eta_4^z = \frac{n_e m_D T_z}{\bar{Z} e B} \quad (17)$$

The plasma mass density can be written

$$n_p m_p \equiv n_i m_i + n_z m_z$$

$$= n_e m_D \left[\frac{\left(\frac{m_i}{m_D}\right) Z + \left(1 - \frac{m_i}{m_D}\right) Z_{eff} - 1}{Z - 1} \right]$$

$$\equiv n_e \bar{m}_D \tag{18}$$

For a deuterium plasma, $\bar{m}_D = m_D$.

2.8. Geometric approximation

To simplify the calculational model, the low beta circular flux surface approximation is used. Non-circular plasmas with horizontal and vertical radii a and b are approximated by a circular plasma with effective radius

$$\bar{a} = \sqrt{ab} = a\sqrt{\frac{b}{a}} \tag{19}$$

which preserves area for an ellipse.

2.9. Profile approximation

Using the geometric approximation of the previous section and the gyroviscous model of Section 2.6, and writing

$$\begin{aligned} n(r) &= n_0 h_n(r) \\ T(r) &= T_0 h_T(r) \\ v_\phi(r) &= v_{\phi 0} h_v(r) \end{aligned} \tag{20}$$

leads to spatial integrals of the form

$$\begin{aligned} (h_{nTv})^{-1} &\equiv \frac{2}{\bar{a}^2} \int_0^{\bar{a}} h_n(r) h_T(r) h_v(r) r dr \\ (h_{nT2v})^{-1} &\equiv \frac{2}{\bar{a}^2} \int_0^{\bar{a}} h_n(r) h_T(r) h_v^2(r) r dr \end{aligned} \tag{21}$$

and so on.

To further simplify the model, radial profiles are represented as parabolas raised to the power α_j, i.e.

$$\begin{aligned} h_n(r) &= (1 - (r^2/a^2))^{\alpha_n} \\ h_T(r) &= (1 - (r^2/a^2))^{\alpha_T} \\ h_v(r) &= (1 - (r^2/a^2))^{\alpha_v} \end{aligned} \tag{22}$$

which leads to the simple forms

$$\begin{aligned} h_{nTv} &= 1 + \alpha_n + \alpha_T + \alpha_v \\ h_{nT2v} &= 1 + \alpha_n + \alpha_T + 2\alpha_v \end{aligned} \tag{23}$$

and so on.

2.10. Computational model

With the gyroviscous model of Section 2.6, the single dominant impurity model of Section 2.7, and the geometric and profile approximations of Sections 2.8 and 2.9, the definitions given in Sections 2.3 to 2.5 reduce to simple formulas suitable for computation.

The rate of gyroviscous torque transfer of Eq. (13) becomes

$$\left\langle R^2 \nabla\phi \cdot \nabla \cdot \vec{\vec{\pi}}_j \right\rangle \simeq -\frac{1}{r} \frac{\partial}{\partial r} \left\langle \eta_4^j R^2 \frac{\partial \Omega_\phi^j}{\partial \theta} \right\rangle \tag{24}$$

As discussed in Sections 2.6 and 2.7, Eq. (24) is evaluated using Eq. (17) for η_4^j, setting $|\partial\Omega_\phi^j/\partial\theta| = \epsilon|\Omega_\phi^j|$ for the dominant impurity species and setting $\partial\Omega_\phi^j/\partial\theta = 0$ for the main ions. Thus, in this model, the radial transfer of angular momentum is due to the dominant impurity species.

Equation (9) becomes

$$\hat{\tau}_\phi^{ex} = \frac{2\pi^2 \bar{a}^2 R_0^3 n_{e0} \bar{m}_D \Omega_{\phi 0}^{ex}}{\Gamma_\phi h_{nv}} \tag{25}$$

The torque input rate from NBI can be computed from

$$\Gamma_\phi = \sqrt{2m_b} \sum_i \frac{R_{Ti} P_{bi}}{\sqrt{E_{bi}}} \left(\frac{\sum_j (f_j/\sqrt{j})}{\sum_j (f_j/j)} \right) \tag{26}$$

where the sum over i is over all ion sources and the sum over j is over the molecular fractions f_j of full, half and third energy components. m_b is the mass of the beam particle, E_{bi} is the energy of the full energy (j = 1) atomic component, P_{bi} is the power delivered by ion source i, and R_{Ti} is the tangency radius of ion source i.

The experimental momentum confinement time of Eq. (8) is rewritten as

$$\tau_\phi^{ex} = \frac{\hat{\tau}_\phi^{ex}}{1 - \beta \hat{\tau}_\phi^{ex}} \tag{27}$$

and the 'acceleration' correction

$$\beta \simeq \frac{1}{N_e}\frac{\partial N_e}{\partial t} + \frac{1}{v_\phi}\frac{\partial v_\phi}{\partial t} \tag{28}$$

can be evaluated using average, total or central quantities, under the assumption that the magnitudes change faster than the profiles.

Note that Eqs (13) and (24) represent the gyroviscous torque transfer as the result of a diffusive process, i.e. in terms of a second-order differential operator acting upon the toroidal velocity. To evaluate Eq. (7), it is assumed that the density and the rotation velocity are each separable in θ and r. The radial profile factor, $-r\,\partial \ln(\eta_4 v_\phi)/\partial r$, is set to unity, and the poloidal profile factor is assumed to be represented by $\partial\Omega_\phi/\partial\theta = \epsilon\Omega_\phi$. The latter assumption is discussed in Section 7.

The theoretical momentum confinement time of Eq. (11) becomes

$$\tau_\phi^{th} = \left(\frac{2R_0^2\bar{Z}eB}{T_{i0}}\right)\left(\frac{h_{nTv}}{h_{nv}}\right)\left(\frac{\bar{m}_D}{m_D}\right) \tag{29}$$

and the theoretical central rotation velocity of Eq. (12) becomes

$$\Omega_{\phi 0}^{th} = \frac{\Gamma_\phi \bar{Z}eB\,h_{nTV}}{\pi^2\bar{a}^2R_0n_{e0}m_DT_{i0}(1+\beta\tau_\phi^{th})} \tag{30}$$

2.11. Velocity decay measurements

A rotation velocity decay constant,

$$(\tau_{decay})^{-1} \equiv -\frac{1}{v_{\phi 0}}\frac{\partial v_{\phi 0}}{\partial t} \tag{31}$$

is sometimes measured after termination of NBI. This decay constant is related, but not equal, to the momentum confinement time. Using the previous approximations,

$$\frac{\dot{L}_\phi}{L_\phi} = \frac{\frac{\partial}{\partial t}\left(\frac{n_{e0}\bar{m}_Dv_{\phi 0}}{h_{nv}}\right)}{\left(\frac{n_{e0}\bar{m}_Dv_{\phi 0}}{h_{nv}}\right)} = \frac{1}{v_{\phi 0}}\frac{\partial v_\phi}{\partial t} + \frac{1}{n_{e0}}\frac{\partial n_{e0}}{\partial t}$$

$$+ h_{nv}\frac{\partial h_{nv}^{-1}}{\partial t} \tag{32}$$

To interpret this decay constant in terms of the momentum confinement time, Eq. (4) — with $\Gamma_\phi = 0$ — Eq. (11) and Eqs (31) and (32) are used to obtain

$$(\tau_{decay})^{-1} = (\tau_\phi^{th})^{-1} + \frac{1}{n_{e0}}\frac{\partial n_{e0}}{\partial t} + h_{nv}\frac{\partial h_{nv}^{-1}}{\partial t} \tag{33}$$

Since the density usually drops rapidly after termination of NBI, Eq. (33) predicts that $\tau_{decay} > \tau_\phi^{th}$. Decay constants are substantially larger than momentum confinement times in experiments where both are measured [3, 6], which is qualitatively consistent with Eq. (33) and a rapidly decreasing density.

3. ROTATIONAL CORRECTIONS TO MEASURED ENERGY CONFINEMENT TIMES

A viscous phenomenon capable of radially transferring momentum at the rate inferred from rotation measurements in tokamaks with unbalanced NBI might also be expected to have some effect on the energy balance and on the energy confinement time.

3.1. Energy balance equation

The total (thermal plus rotational) energy balance on the plasma is given by

$$\dot{W}_{rot} + \dot{W}_{th} + H_Q = P_{TOT} - P_{RAD} \tag{34}$$

where

$$W_{rot} \equiv \int_{\psi_0}^{\psi_a} \left\langle \tfrac{1}{2}nmv^2 \right\rangle V'(\psi)d\psi \tag{35}$$

is the rotational energy,

$$W_{th} \equiv \int_{\psi_0}^{\psi_a} \left\langle \tfrac{3}{2}p + E_f \right\rangle V'(\psi)d\psi \tag{36}$$

is the thermal energy, including 'background' plasma ions and electrons $\left(\frac{3}{2}p\right)$ and 'fast' beam ions in the process of thermalizing (E_f),

$$P_{TOT} \equiv P_{NB} + P_{RF} + P_{OH} \tag{37}$$

is the total power input to the plasma from NBI, RF heating and Ohmic heating, P_{RAD} is the radiated power from the central confinement region, and

$$H_Q \equiv \int_{\psi_0}^{\psi_a} \langle \nabla\cdot\vec{Q} \rangle V'(\psi)d\psi \tag{38}$$

is the total (thermal plus kinetic) energy flowing out of the confinement region.

The textbook definition (e.g. [9]) of the total energy flux is

$$\vec{Q} \equiv \left\{\left(\tfrac{1}{2}nmv^2 + \tfrac{5}{2}p\right)\vec{v} + \vec{q}\right\} + \left\{\vec{v}\cdot\vec{\vec{\pi}}\right\} \equiv \vec{Q}_c + \vec{Q}_\pi \tag{39}$$

where $\vec{q}$ is the heat conduction, $\frac{3}{2}p\vec{v}$ is the convection of thermal energy, $\frac{1}{2}nmv^2\vec{v}$ is the convection of kinetic (rotation) energy, and $\vec{v}\cdot\vec{\vec{P}} \equiv p\vec{v} + \vec{v}\cdot\vec{\vec{\pi}}$ is the work done by the rotating plasma against the restraining pressure tensor. The first and fourth terms in Eq. (39) are usually neglected because of ordering arguments that rely upon $v \sim \delta v_{th} \ll v_{th}$ which are valid for non-rotating plasmas. However, these terms must be retained for plasmas in which some species are rotating with speeds $v_\phi \simeq v_{th}$. The first { } in Eq. (39) collects terms associated with conductive and convective processes, and the second { } contains the effective outward kinetic (rotational) energy flux associated with work done against viscous stress. The convection and conduction of energy associated with the fast beam ions is implicitly included in the first { } in Eq. (39).

If energy is transported out of the confinement region to the edge of the plasma and then partially converted to radiative energy in the edge region, including it in the global energy balance would be 'double counting'. For simplicity, it is assumed that all radiation emanates from the edge of the plasma, in which case $P_{RAD} = 0$.

3.2. Experimental energy confinement time

The most commonly used definition of energy confinement time is in terms of the *thermal* (heat) energy replacement rate

$$\tau_E^{ex} \equiv \frac{W_{th}}{P_{TOT} - \dot{W}_{th}} \tag{40}$$

It is worth noting that a more natural definition might be given in terms of the *total* energy replacement rate:

$$(\tau_E^{ex})' \equiv \frac{W_{th} + W_{rot}}{P_{TOT} - (\dot{W}_{th} + \dot{W}_{rot})} \tag{41}$$

However, the definition is not so important as the consistency between definitions of experimental and theoretical confinement times, and Eq. (40) is used here in order to be in agreement with common usage.

3.3. Theoretical energy confinement time

To obtain a consistent expression for a theoretical confinement time for comparison with Eq. (40), Eq. (34) is used to replace $P_{TOT} - \dot{W}_{th}$ in the denominator of Eq. (40), with $H_Q + \dot{W}_{rot}$ ($P_{RAD} = 0$), to obtain

$$(\tau_E^{th})^{-1} \equiv \frac{H_Q + \dot{W}_{rot}}{W_{th}}$$

$$\equiv (\tau_{EC})^{-1} + (\tau_{E\pi})^{-1} + (\tau_{EA})^{-1} \tag{42}$$

where

$$\tau_{EC}^{-1} \equiv \frac{\int_{\psi_0}^{\psi_0} \langle\nabla\cdot\vec{Q}_c\rangle V'(\psi)d\psi}{W_{th}} \tag{43}$$

is the energy confinement time associated with all conductive and convective processes (neoclassical plus anomalous),

$$\tau_{E\pi}^{-1} \equiv \frac{\int_{\psi_0}^{\psi_a} \langle\nabla\cdot\vec{Q}_\pi\rangle V'(\psi)d\psi}{W_{th}} \equiv \frac{H_{Q\pi}}{W_{th}} \tag{44}$$

is the energy confinement time associated with the work done by the rotating plasma against viscous stress, or with the effective viscous flux of rotational energy, and

$$\tau_{EA}^{-1} \equiv \frac{\dot{W}_{rot}}{W_{th}} \tag{45}$$

is an acceleration correction term. Equations (44) and (45) can be combined to obtain an effective 'rotational' confinement time

$$(\tau_{E\Omega})^{-1} \equiv (\tau_{E\pi})^{-1} + (\tau_{EA})^{-1} \tag{46}$$

which would be infinite in a non-rotating plasma, but becomes finite and affects the overall energy confinement time — see Eq. (42) — in a strongly rotating plasma.

3.4. Conductive–convective energy confinement time

To obtain an experimental confinement time which can be compared with theoretical predictions for energy

confinement against conductive and convective processes, it is necessary to correct the measured confinement time calculated from Eq. (40) using measured quantities. Equating τ_E^{ex} of Eq. (40) with τ_E^{th} of Eq. (42) leads to an expression for the experimental value of the energy confinement time against conductive and convective processes (neoclassical and anomalous):

$$\tau_{EC}^{ex} = \frac{\tau_E^{ex}}{1 - \tau_E^{ex}/\tau_{E\Omega}} \tag{47}$$

in terms of the quantity constructed from measurement, τ_E^{ex}, and the rotational energy confinement time, $\tau_{E\Omega}$ of Eq. (46).

Assuming, for the moment, that $\tau_{E\Omega} > 0$, which turns out to be the case (see Section 3.8), Eq. (47) shows that the energy confinement time against conductive and convective processes is larger than the experimental energy confinement time measured in a strongly rotating plasma.

3.5. Energy confinement degradation due to rotation

Equation (42) can be rearranged to yield

$$\tau_E = \frac{\tau_{EC}}{1 + \tau_{EC}/\tau_{E\Omega}} \tag{48}$$

Provided that $\tau_{E\Omega} > 0$, which is the case, Eq. (48) predicts a degradation of energy confinement due to rotational-viscous and acceleration effects in a strongly rotating plasma, even if the conductive-convective processes are not affected by the NBI that produces the rotation.

3.6. Relationship between $\tau_{E\pi}$ and τ_ϕ

There is an intrinsic relationship between $\tau_{E\pi}$ and τ_ϕ^{th} arising from the fact that both are defined in terms of the same viscous stress tensor, independent of the mechanism responsible for the viscous stress. From Eqs (11) and (44),

$$\frac{\tau_{E\pi}^{-1}}{\tau_\phi^{-1}} \equiv \frac{L_\phi}{W_{th}} \cdot \frac{H_{Q\pi}}{\pi_\phi} = 4\left(\frac{W_{rot}}{W_{th}}\right)\left(\frac{h_{n2v}h_\pi}{h_{nv}h_{v\pi}}\right) \tag{49}$$

The geometric approximation of Section 2.8 and the profile representation of Eqs (20) and a similar representation for the radial profile of π have been used in deriving the last form of Eq. (49). When the rotational speed of the main plasma ion species approaches about one-half of the thermal speed, $(v_\phi^i \sim \frac{1}{2}v_{th}^i)$, the magnitude of $\tau_{E\pi}^{-1}$ becomes comparable to the magnitude of τ_ϕ^{-1}. In such plasmas, the correction to the measured energy confinement time described in Section 3.4 and the degradation of energy confinement time due to rotation described in Section 3.5 are comparable in magnitude to the observed inverse momentum confinement times.

3.7. Viscous energy flux model

Using the gyroviscous model [8] for the viscous stress, the viscous energy flux across flux surfaces can be written

$$\langle(\nabla\cdot\vec{Q}_{\pi j})_\psi\rangle = -\left\langle \frac{1}{Rh_p}\frac{\partial}{\partial \ell_\psi}\left(R^3 h_p \eta_4^j \Omega_\phi^j \frac{\partial \Omega_\phi^j}{\partial \ell_p}\right)\right\rangle \tag{50}$$

Comparing Eqs (13) and (50), or Eqs (24) and (51), it is seen that the radial component of the divergence of the viscous energy flux, which enters the energy confinement time, is identical, except for an additional Ω_ϕ, with the toroidal component of the viscous torque (momentum transfer rate), which determines the theoretical momentum confinement time. Thus, agreement between theoretical and experimental momentum confinement times would also serve as a confirmation of the gyroviscous energy confinement time computed from Eq. (44) by inserting Eq. (50).

There are several components of the viscous energy flux: $\vec{v}\cdot\vec{\vec{\pi}} = v_\psi\pi_{\psi\psi} + v_p\pi_{p\psi} + v_\phi\pi_{\phi\psi}$. Only the last component, $v_\phi\pi_{\phi\psi}$, is included in Eq. (50) and in the subsequent development. This term involves the same tensor element, $\pi_{\phi\psi}$, that is involved in the momentum confinement time, hence providing the means for experimental confirmation. It can be shown that $|\pi_{p\psi}| \ll |\pi_{\phi\psi}|$. For the purpose of this paper, the $v_\psi\pi_{\psi\psi}$ terms,which are estimated to be small, may be considered to be lumped into the convective component of the heat flux.

3.8. Computational model

Use of the geometrical and profile approximations of Sections 2.8 and 2.9 and the single dominant impurity model of Section 2.7 allows simple formulas to be obtained which are convenient for computation. The viscous energy flux of Eq. (50) becomes

$$\langle(\nabla\cdot\vec{Q}_{\pi j})\rangle = -\left\langle \frac{1}{r}\frac{\partial}{\partial r}\left(\eta_4^j R^2 \Omega_\phi^j \frac{\partial \Omega_\phi^j}{\partial \theta}\right)\right\rangle \tag{51}$$

For the dominant impurity species, Eq. (17) is used to evaluate η_4^j, with $|\partial\Omega_\phi^j/\partial\theta| = \epsilon|\Omega_\phi^j|$. For the main ion species, $\partial\Omega_\phi^j/\partial\theta = 0$ is used. Thus, the viscous energy flux in this model is due entirely to impurities. The confinement time associated with this viscous energy flux, defined by Eq. (44), reduces to

$$\tau_{E\pi}^{-1} = \left(\frac{2\pi^2\bar{a}^2R_0n_{e0}T_{i0}}{W_{th}h_{nT2v}}\right)\left(\frac{\Omega_{\phi0}^2}{\bar{Z}eB/m_D}\right) \tag{52}$$

and the confinement time associated with acceleration, defined by Eq. (45), reduces to

$$\tau_{EA}^{-1} = \frac{2\pi^2\bar{a}^2R_0\left(\frac{1}{2}n_{e0}\bar{m}_Dv_{\phi0}^2\right)}{W_{th}h_{n2v}} \cdot \gamma \tag{53}$$

where

$$\gamma \equiv \frac{\dot{W}_{rot}}{W_{rot}} \simeq \frac{1}{N_e}\frac{\partial N_e}{\partial t} + 2\frac{1}{v_\phi}\frac{\partial v_\phi}{\partial t} \tag{54}$$

Assuming that magnitudes change faster than profiles, central, average or total values can be used to evaluate Eq. (54).

From Eqs (46), (52) and (53) it is seen that $\tau_{E\Omega} \sim 1/\Omega_{\phi0}^2 > 0$. Thus, the rotational effect will always be such as to cause the measured energy confinement time in a strongly rotating plasma to be less than the energy confinement time against conductive and convective processes, Eq. (47), and to produce a degradation in the measured energy confinement time, Eq. (48). Both effects vary as $\Omega_{\phi0}^2$.

The relative magnitudes of the acceleration and viscous inverse confinement times are

$$\frac{\tau_{EA}^{-1}}{\tau_{E\pi}^{-1}} = \gamma\left(\frac{1}{2}\frac{\bar{Z}eBR_0}{T_{i0}}\right)\left(\frac{\bar{m}_D}{m_D}\right)\left(\frac{h_{nT2v}}{h_{n2v}}\right) \tag{55}$$

which is $\sim(10^{-1} - 10^{-2})\gamma$ for most plasmas of current interest. Thus, the acceleration correction is expected to be only $\sim$1–10% of the inverse rotational confinement time defined by Eq. (46), assuming $\gamma \lesssim 1$.

Using Eqs (29) and (52), Eq. (49) is recovered, but now with the explicit forms $h_\pi = h_{nTv}$ and $h_{v\pi} = h_{nT2v}$.

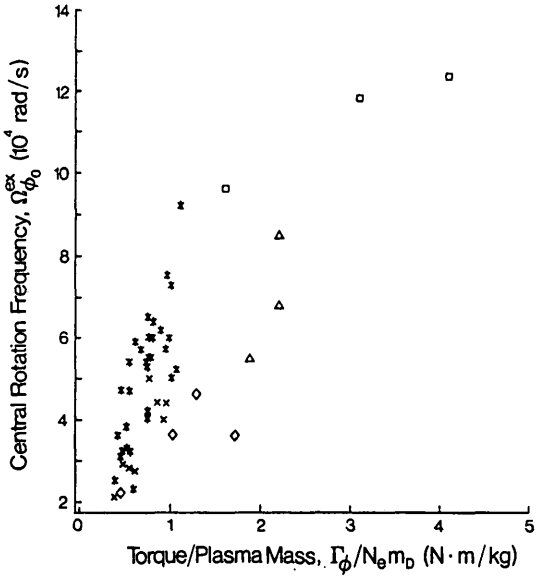

FIG. 1. Experimental central rotation frequencies in JET.
** — H-mode, NBI only; × — H-mode-like, NBI + ICRF;*
△ — L-mode, NBI only; ◇ — L-mode, NBI + ICRF;
□ — L-mode 'jolly good' shots.

4. APPLICATION TO JET

4.1. JET rotation measurements

Rotation velocities are measured in JET by two methods. An X-ray crystal spectrometer [15] views radiation from a Ni XXVII resonance line, which allows the determination of the toroidal angular velocity of the central region of the plasma, where this charge state is concentrated, via a Doppler shift determination. More recently, a multi-chordal visible charge exchange recombination spectroscopy (CXRS) diagnostic [16] has produced radial profiles of the toroidal velocities of the dominant light impurities (carbon and oxygen). Both measurements agree to within the experimental error [17].

A subset of the JET rotation data [18] has been chosen for an application of the analysis methods of the previous two sections. This subset consists of the discharges during the first eight months of 1988, for which the CXRS diagnostic was used to obtain rotation profiles that were processed and placed in the JET processed physics file (PPF). H-mode and L-mode discharges, discharges with NBI only, and discharges with NBI plus substantial RF heating, X-point and limiter discharges, and elongated ($K \simeq 1.6$–1.8) and nearly circular discharges were included. In JET, a rapid and substantial density increase is associated with NBI, so that, for H-mode discharges, the rotation velocity peaks and then decreases before the thermal energy content reaches its maximum value. For such shots, observations at both the maximum rotation

velocity and the maximum energy were included in the analysis. Care was taken to avoid times when a sawtooth crash had produced a reduction in the central rotation velocity [7]. Some discharges were rejected because of erratic functioning of the ion sources or of an important (to this analysis) diagnostic. A small number of discharges with large NBI power but very small rotation velocities were rejected because some other momentum transfer mechanism was obviously dominant. The observations selected for analysis were from deuterium discharges; these are characterized in Fig. 1, where the measured central rotation frequency is plotted versus the beam torque per plasma mass. The NBI powers varied over the range $4 < P_b < 15$ MW, the central ion temperature varied over the range $3.5 \leq T_{i0} \leq 17.5$ keV, and the central electron densities varied over the range $2.5 < n_{e0} < 8.2 \times 10^{19}$ m^{-3}. The plasma current was slightly higher than 3 MA in all discharges, and the toroidal magnetic field took on a few discrete values in the range $2.2 < B_\phi < 3.5$ T. Z_{eff} varied over the range $2 \leq Z_{eff} < 4$. The velocity and temperature profiles varied among the discharges from parabolic to somewhat more peaked than parabolic to the fourth power, and the density profiles varied from flat or hollow, for H-mode discharges, to parabolic squared. For most discharges, the major radius (magnetic axis) was in the range $3.0 < R < 3.1$ m, and the horizontal plasma radius was ~ 1.1 m, although some smaller discharges were included.

Five different types of JET discharges are distinguished in Fig. 1 and in the subsequent figures. The symbol * denotes a typical H-mode discharge with only NBI — these discharges are characterized by a reduced H_α signal and by a flat or hollow electron density profile. The symbol × denotes a discharge with NBI and ICRF which is H-mode-like in that it has a flat or hollow density profile, but which does not, except in one case, have a distinctly reduced H_α signal. The symbol Δ denotes typical L-mode discharges with a peaked density profile and a large H_α signal, with NBI only. The symbol ◇ denotes L-mode discharges with NBI and ICRF. The symbol □ denotes a series of low density, high NBI power discharges in smaller, nearly circular plasmas that were intended to simulate the TFTR 'supershot' regime, referred to as 'jolly good' shots.

One of the assumptions made in developing the model in Section 2 was that $|\partial\Omega_\phi/\partial\theta| = \epsilon|\Omega_\phi|$, more specifically that an up–down poloidal asymmetry [8] in Ω_ϕ of $O(\epsilon)$ existed, for the dominant impurity species. Ω_ϕ is measured as a function of horizontal position for the dominant impurity (carbon) in JET. From these measured radial profiles it is possible, in principle, to determine any horizontal asymmetry, but not any vertical asymmetry. The existence of an $O(\epsilon)$ horizontal asymmetry would tend to support, but not confirm, this aspect of the theoretical model. The measured Ω_ϕ profile was mapped onto flux surface co-ordinates determined by the IDENTC equilibrium code for several pulses. A poloidal asymmetry in Ω_ϕ in the range $\sim \frac{1}{2}\epsilon < \Delta\Omega_\phi/\Omega_\phi < \epsilon$ was found. Since the data are not available in the PPF to perform a systematic error analysis and since only a limited number of pulses were examined, this result must be considered as inconclusive. A more definitive analysis of this point would be of substantial value.

A poloidal asymmetry in Ω_ϕ is consistent with results reported previously for JET [17], but is at variance with the result reported for D-III [4], where CXRS was used to determine the rotation frequency of He and it was found that Ω_ϕ was uniform over the flux surface to within the experimental error. This difference in the results is not inconsistent with theory [13], which predicts that Ω_ϕ has an $O(\epsilon)$ variation for ions rotating at speeds comparable to their thermal speeds but has a much smaller variation for ions rotating much slower than their thermal speed. Since it is the inertial effect which drives the variation to $O(\epsilon)$, the magnitude of the variation scales as $(v_\phi/v_{th})^2$. Helium in D-III was rotating at a small fraction of its thermal speed and hence the variation in Ω_ϕ would be expected to be much less than $O(\epsilon)$, as reported. Carbon in JET was rotating at speeds comparable to its thermal speed and hence the variation in Ω_ϕ would be expected to be $O(\epsilon)$, as found.

These experimental results certainly do not provide a verification of $O(\epsilon)$ vertical asymmetries in rotation frequency for impurities, nor do they refute them. Experimental attention to this matter would be most valuable.

4.2. Modelling of the JET experiments

The computational formulas given in Sections 2.10 and 3.8 were used. All parameters were evaluated from processed experimental data (PPF). Parabolas to a power were fitted to measured density, temperature and velocity profiles. Central values were set equal to the maximum measured values, which occurred near, but not at, the magnetic axis for T_i and Ω_ϕ, except for n_{e0} in H-mode discharges. For H-mode discharges in JET the density profile is very flat or hollow, in which case $\alpha_n = 0$ was used and n_{e0} was chosen to preserve the total number of particles. Horizontal and vertical

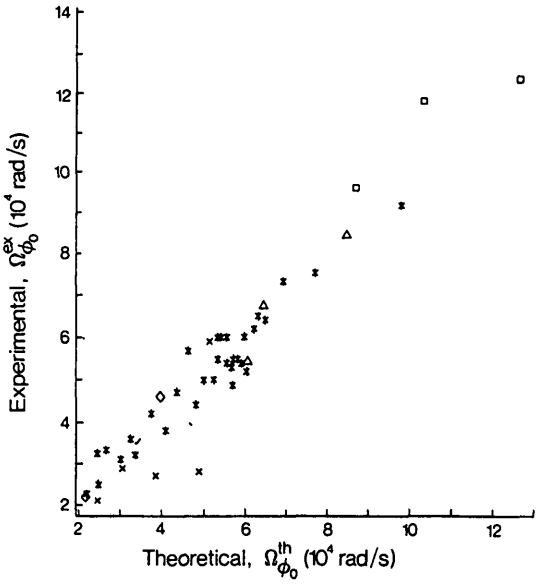

FIG. 2. Comparison of experimental and theoretical central angular rotation frequencies in JET.
** — H-mode, NBI only; × — H-mode-like, NBI + ICRF;*
Δ — L-mode, NBI only; ◇ — L-mode, NBI + ICRF;
□ — L-mode 'jolly good' shots.

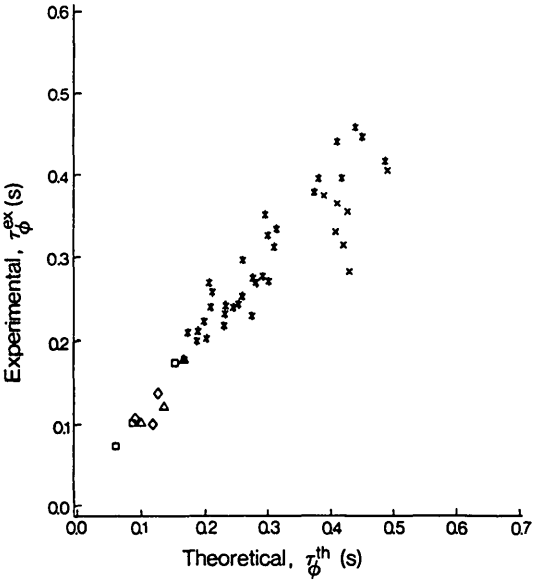

FIG. 3. Comparison of experimental and theoretical momentum confinement times in JET.
** — H-mode, NBI only; × — H-mode-like, NBI + ICRF;*
Δ — L-mode, NBI only; ◇ — L-mode, NBI + ICRF;
□ — L-mode 'jolly good' shots.

scans of visible bremsstrahlung were used to determine Z_{eff}. When the two valves differed, which was the norm, neoclassical resistivity measurements, comparison with other pulses in a sequence, etc. were also used to select a value for Z_{eff}.

The neutral beam system in JET [11] has 16 different ion sources, eight oriented with tangency radius 1.85 m and eight oriented with tangency radius 1.18 cm. Different combinations of sources were used in different discharges, requiring Eq. (27) to be evaluated for each discharge. The molecular fractions in the beam were $f_1 = 0.75$, $f_2 = 0.16$, $f_3 = 0.09$, and a maximum beam energy of $E_b = 80$ keV was used.

4.3. Central rotation frequency and momentum confinement time

The measured and calculated central rotation frequencies and momentum confinement times are compared in Figs 2 and 3, respectively. There is good agreement. The agreement is poorest for H-mode-like discharges which have ICRF heating in addition to NBI; the theory overpredicts the rotation frequency by as much as a factor of two and overpredicts the momentum confinement times by ~30%. This is consistent with the earlier observation [7] that ICRF heating caused a sharp drop in rotation velocity and suggests that ICRF heating introduces an additional momentum loss mechanism in JET.

The low density, high power 'jolly good' shots, with velocity profiles that are parabolic to the fourth power or greater, obtained the highest rotation frequencies. The H-mode and H-mode-like discharges generally had larger momentum confinement times than the L-mode discharges. The momentum confinement times for the H-mode and L-mode discharges were mainly in the ranges 200–500 ms and 100–200 ms, respectively. The energy confinement times for the same discharges (see Fig. 6) are in the ranges 600–1000 ms and 350–600 ms for H-mode and L-mode discharges, respectively.

This analysis should be considered as illustrative, rather than comprehensive. Only part of the rapidly expanding JET rotation database was included. A comprehensive compilation and analysis activity has been initiated [18].

4.4. Parameter dependence of $\Omega^{ex}_{\phi 0}$ and τ^{ex}_{ϕ}

It is not possible to make a definitive check of the dependence of $\Omega^{ex}_{\phi 0}$ or τ^{ex}_{ϕ} on an experimental parameter A simply by plotting $\Omega^{ex}_{\phi 0}$ or τ^{ex}_{ϕ} against parameter A,

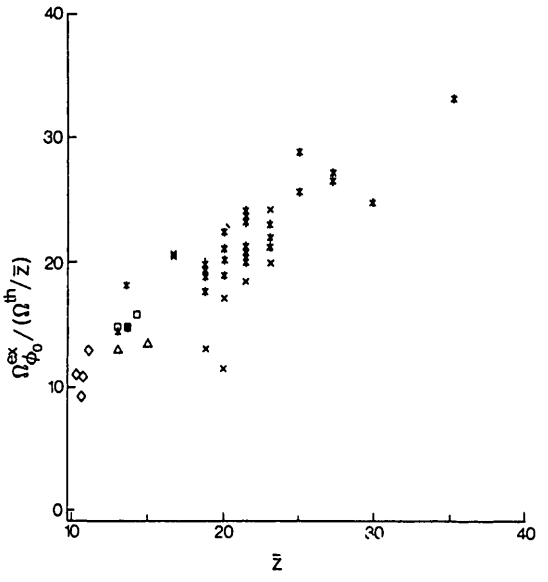

FIG. 4. Scaling of the experimental central angular rotation frequency with the parameter $\bar{Z}$ in JET.
** — H-mode, NBI only; × — H-mode-like, NBI + ICRF;*
△ — L-mode, NBI only; ◇ — L-mode, NBI + ICRF;
□ — L-mode 'jolly good' shots.

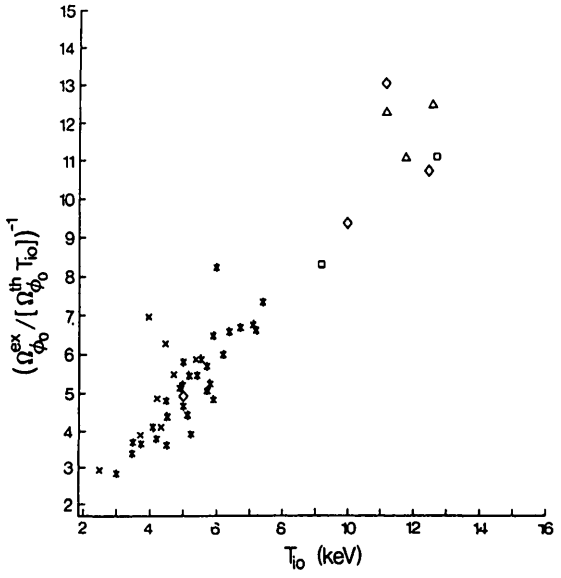

FIG. 5. Scaling of the experimental central angular rotation frequency with the central ion temperature in JET.
** — H-mode, NBI only; × — H-mode-like, NBI + ICRF;*
△ — L-mode, NBI only; ◇ — L-mode, NBI + ICRF;
□ — L-mode 'jolly good' shots.

because $\Omega^{ex}_{\phi 0}$ or τ^{ex}_{ϕ} surely depend upon other parameters that also vary among discharges at different values of A. However, it is possible to check whether the measured $\Omega^{ex}_{\phi 0}$ or τ^{ex}_{ϕ} has the parameter dependence predicted by theory, in this case the gyroviscous theory. For example, if $\Omega^{ex}_{\phi 0}$ has the dependence upon $\bar{Z}$ given by theory (Eq. (29)), then it should be possible to divide $\Omega^{ex}_{\phi 0}$ by $\Omega^{th}_{\phi 0}$ of Eq. (29), but with $\bar{Z}$ suppressed, and to obtain a quantity $\Omega^{ex}_{\phi 0}/(\Omega^{th}_{\phi 0}/\bar{Z})$ which varied linearly as Z. Similarly, the quantity $(\Omega^{th}_{\phi 0} T_{i0})/\Omega^{ex}_{\phi 0}$ should vary linearly with T_{i0} if the experimental data have the parameter dependence predicted by Eq. (29). Such plots are shown in Figs 4 and 5, where the predicted parameter dependence on $\bar{Z}$ and T_{i0} is seen to be found in the data. Similar results were obtained for τ^{ex}_{ϕ}. There are not sufficient variations in other parameters (e.g. B, R) in the pulses analysed to provide a similar check.

We note that the procedure used here checks a necessary, but not sufficient, condition for the data to exhibit the parameter dependence predicted by theory. It is possible that the coincidence of calculated and measured quantities is due either to a dependence of the latter on some other parameters which are correlated with the parameters in the theoretical formula or to purely random causes, but these possibilities are considered to be unlikely.

4.5. Energy confinement time

The experimental energy confinement time constructed from Eq. (40) for the same set of observations is plotted in Fig. 6. The characteristic degradation of τ_E with input power is apparent. The interesting question is: what part of this degradation is associated with rotational effects and what part is associated with enhanced conductive and convective (neoclassical and anomalous) processes? Equation (47) can be used to compute the fraction of the total energy loss rate that is due to conductive and convective processes:

$$\left(\frac{\tau^{ex}_E}{\tau^{ex}_{EC}}\right) = 1 - \tau^{ex}_E/\tau_{E\Omega}$$

and Eqs (46), (52) and (53) can be used to evaluate $\tau_{E\Omega}$. The result is plotted in Fig. 7. For the discharges with $\Omega_{\phi 0} \geq 10^5$ rad/s, approximately 25% of the total energy loss rate is associated with rotational effects (primarily the gyroviscous energy flux — the acceleration correction is $<10\%$). If NBI did not also enhance the conductive and convective loss rate, this rotational effect would enhance the total loss rate by about one third relative to the non-rotating (Ohmic) value, which would

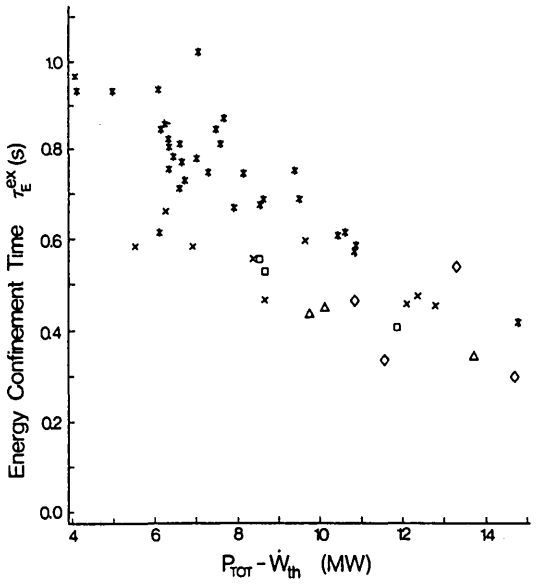

FIG. 6. Experimental energy confinement times in JET.
** — H-mode, NBI only; × — H-mode-like, NBI + ICRF;*
Δ — L-mode, NBI only; ◇ — L-mode, NBI + ICRF;
□ — L-mode 'jolly good' shots.

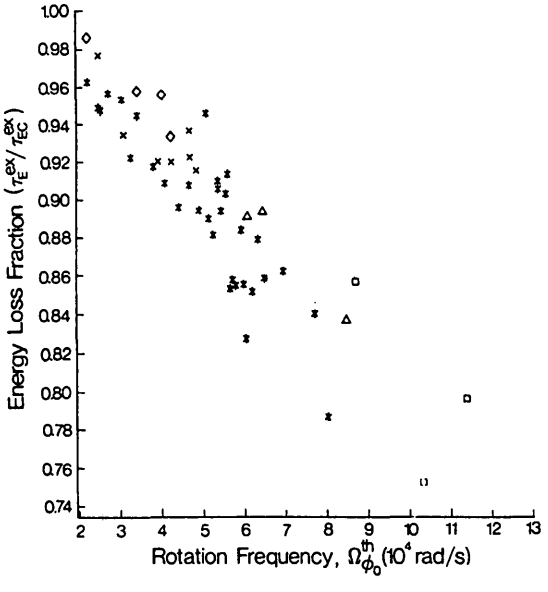

FIG. 7. Conductive-convective fraction of the total energy loss in JET.
** — H-mode, NBI only; × — H-mode-like, NBI + ICRF;*
Δ — L-mode, NBI only; ◇ — L-mode, NBI + ICRF;
□ — L-mode 'jolly good' shots.

correspond to degradation of energy confinement of about 25% in the most extreme (fastest rotating) cases considered. The measured energy confinement times are degraded by about 50% for these discharges, so that the rotational effects can account for about half of the degradation.

Since the same basic mechanisms for momentum transfer (gyroviscosity in this paper) is involved in the theoretical models for τ_ϕ and $\tau_{E\pi}$, the agreement between theory and experiment for τ_ϕ gives a corresponding measure of confidence in the predictions of $\tau_{E\pi}$.

5. APPLICATION TO THE TFTR BEAM POWER SCAN

There is a large body of data in the literature on energy confinement degradation with unbalanced NBI. The TFTR beam power scan experiments [19] were chosen because:

- they are representative of the published TFTR L-mode data;
- they are well documented (all parameters needed to evaluate the theory are available for all shots);
- they were carefully controlled (a minimal number of parameters other than those of interest varied among shots);
- both energy confinement and momentum confinement data were available;
- the predicted gyroviscous energy confinement degradation was large enough to be observed experimentally; and
- the analysis of a beam power scan illustrates some different aspects of the formalism given in Sections 2 and 3.

5.1. TFTR beam power scan measurements

The dedicated beam power scan data in Ref. [19] are well suited to test the extent to which the rotational effect can quantitatively account for the degradation of energy confinement time with beam power. This set of experiments is well documented and the momentum confinement times have also been measured [6], so that the gyroviscous theory of momentum confinement can be compared with the same set of experiments as a further confirmation. The beam power scan experiments consisted of a series of shots which were run in a deuterium plasma in which the final density ($\bar{n}_e = 4.6 \times 10^{19}$ m^{-3}), the magnetic field ($B_\phi = 4.7$ T),

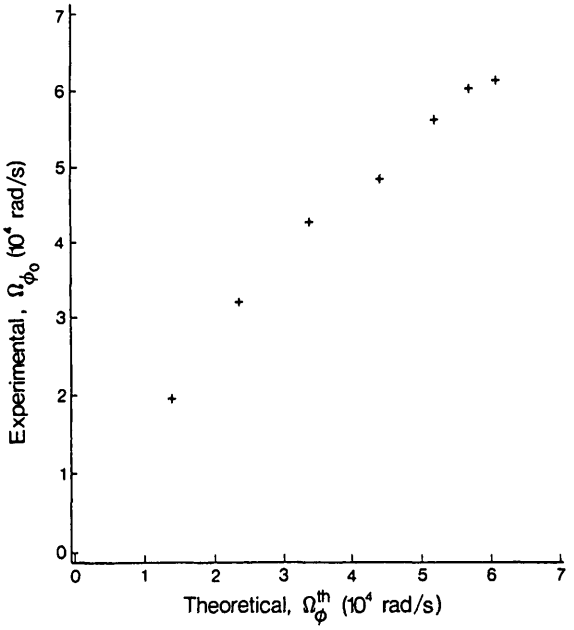

FIG. 8. Comparison of experimental [6] and theoretical central angular rotation frequencies in a TFTR beam power scan.

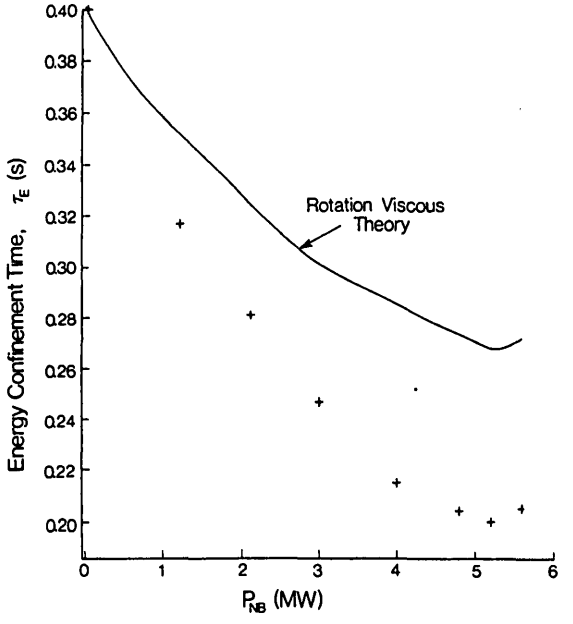

FIG. 9. Degradation of the energy confinement time in a TFTR beam power scan. Comparison of the experimental [20] value (+) with theoretical degradation due to gyroviscous effect (−) alone.

the major radius (R_0 = 2.58 m) and the minor radius (a = 0.82 m), and the plasma current (I = 2.2 MA) were held constant. The deuterium neutral beam power P_b was varied from 1.2 MW to 5.6 MW. The measured Z_{eff} varied from 2 to 3 over this range of beam power. The measured value of the central ion temperature varied linearly from 2.5 keV (P_b = 0) to 4.8 keV (P_b = 5.6 MW). The central rotation velocity was measured from the Doppler shift of the Ti XXI K_α line to vary as $v_\phi(0) = 3.0 \times 10^4 + 2.35 \times 10^4 P_b$ (MW). The energy confinement time, defined as the ratio of the stored thermal energy to the power input, was measured in this scan.

5.2. Modelling of the TFTR beam power scan

The experimental parameters cited in the previous section were used. The radial profiles were assumed to be parabolic ($\alpha_n = \alpha_T = \alpha_v = 1.0$), in the absence of any profile information. The beam torque was calculated for a maximum beam species energy of 80 keV, a species mix of 0.265/0.329/0.406 [10], and a tangency radius equal to the major radius. The plasma ion density was then taken from transport modelling calculations [10].

In these TFTR discharges, steady state conditions were obtained, so that acceleration corrections were unnecessary.

5.3. Central rotation frequency

In Fig. 8, the measured central rotation frequency is compared with the theoretical value; the agreement is good. There is similar good agreement in the experimental and theoretical momentum confinement times, which are about 100 ms.

5.4. Energy confinement degradation

Taking τ_{EC} = 0.4 s as the measured energy confinement time, with P_b = 0, the degradation that would be caused by the gyroviscous energy flux effect alone, assuming τ_{EC} = const., was then calculated from Eq. (48). The result is compared with the measured energy confinement time in Fig. 9. The rotational gyroviscous energy loss is seen to account for about one half of the degradation in energy confinement.

6. DISCUSSION OF RELATED WORK

6.1. ISX-B experiments and analysis

An extensive set of central rotation velocity measurements, including a number of parameter dependences, was made on ISX-B [3]. The analysis, based on gyroviscous theory for the transfer of input torque, was able to explain these data [12].

There are other ISX-B data which appear to contradict the predictions of the gyroviscous theory for energy confinement degradation. An extensive set of experiments in ISX-B [20] with balanced and unbalanced injection led to the conclusion that rotation was not a major cause of energy confinement degradation. In these experiments, the energy confinement time was degraded from ~25 ms to ~5 ms with 0.5–1.5 MW balanced NBI. In a comparison of energy confinement time measurements with unbalanced injection of the same magnitude, a ~25% scatter in the data about the balanced injection value was found, but no definite trend. Taking τ_{EC} = 5 ms to account for all non-rotational effects (including the enhanced conductive-convective loss), assuming parabolic profiles and taking parameters appropriate to ISX-B (B = 1.4 T, $v_\phi = 1 \times 10^5$ m/s, R = 0.93 m, Z_{eff} = 1.5) leads to the prediction that energy confinement with unbalanced injection should be degraded by ~12% relative to balanced injection, which is within the scatter of the data. Thus, the gyroviscous rotational effect is too small to have been detected in ISX-B.

6.2. D-III experiments and analysis

Rotation velocity profiles were measured [4] in D-III, with up to 6.3 MW of NBI producing central rotation velocities in excess of 10^5 m/s. Experimental momentum confinement times in the range of 25–50 ms were obtained, and theoretical estimates [4], based on a version [12] of the gyroviscous model without profile effects, were in the range of 15–30 ms.

In the D-III discharges, the velocity and density profiles flattened as the plasma current was increased. Burrell et al. [4] found that although the central rotation velocity remained approximately constant as the plasma current increased, the angular momentum content increased as the current increased because of the broadening of the density and velocity profiles. This led them to conclude that the experimental momentum confinement time increased with plasma current, as would be predicted by Eq. (25) in which profile broadening would be reflected by a decreasing h_{nv}. The theoretical formula used by these authors did not include profile effects — it consisted of the first term in Eq. (29), but with T_{i0} replaced by T_{av}. As the current increased, T_{av} increased because of better confinement, leading these authors to conclude that the momentum confinement time decreased with increasing plasma current, contrary to the experimental result. From Eq. (29), a broadening of the temperature profile as well as of the density and velocity profiles would cause an increase in the theoretical momentum confinement time. Thus, had these authors accounted for profile effects in the theoretical prediction in the same manner as they did in the experimental definition, they might have found better agreement in the scaling with plasma current.

6.3. TFTR experiments and analysis

Compilation and analysis of an extensive rotation database, on the basis of X-ray crystal spectrometer measurements of Doppler shifted resonance radiation lines and with charge exchange recombination spectroscopy measurements, is in progress for TFTR [5, 6, 21, 22, 23]. Central rotation velocities in excess of 10^6 m/s have been obtained. Initial analyses [5, 6], which did not include any information about velocity profiles, found a rough agreement (to within a factor of three at the worst) between experimental and theoretical (gyroviscous) momentum confinement times. Straightforward plotting of the measured momentum confinement times against the various parameters of the gyroviscous theory did not reveal the parameter dependences predicted by theory, possibly because whatever dependences were present were masked by simultaneous variations in other dependent variables. A more detailed analysis [22, 23] of parts of this dataset finds better agreement (to within a factor of two at the worst) between measured and theoretical central rotation velocities and momentum confinement times, and an examination of the parameter dependences in the experimental data using the method described in Section 4.4 shows the dependence on Z_{eff} and T_{i0} that are predicted by the gyroviscous theory. Analysis [23] of a recent set of dedicated rotation experiments yielded very good agreement.

Extensive studies of the effect of balanced and unbalanced NBI on energy confinement have been carried out on TFTR. In summarizing the L-mode comparison, the authors [24] state "... the difference in τ_E between balanced and co-only injection at P_b = 10 MW is less than 15%", which is much less than the ~30% degradation due to rotational gyro-

viscous losses at $P_b = 5$ MW in the TFTR beam power scan discussed in Section 5.4. On the other hand, in the 'supershot' regime in TFTR, the energy confinement time does not degrade with balanced NBI (no significant rotation) but degrades significantly with unbalanced injection (significant rotation) [24], which is in qualitative agreement with the prediction of Eq. (48) and with the gyroviscous energy flux model which predicts that the confinement time degradation should vary as $(1 + Cv_\phi^2)^{-1}$.

6.4. JET experiments and analysis

An extensive rotation dataset, based on X-ray crystal spectrometer and charge exchange recombination spectrometer and charge exchange recombination spectrometer measurements, is in the process of being compiled and analysed for JET [7, 17, 18]. Comparison [7] of early measurements of central rotation velocities from the X-ray crystal spectrometer, for which no profile information was available, with an earlier formulation [12] of the gyroviscous theory yielded rather good agreement when the full torque delivered by NBI was included in the calculation.

7. GYROVISCOUS THEORY

There is an unresolved controversy regarding one aspect of the gyroviscous theory of momentum transport that is used in this paper. Thus in establishing the context within which the results of this paper should be considered, it is helpful to discuss gyroviscous theory and the current controversy.

The theory of gyroviscous momentum transport was developed originally by Braginskij [25] and Kaufman [26]. Later, Stacey and Sigmar [8] extended the theory to flux surface and toroidal geometries and demonstrated that the magnitude of the gyroviscous force was proportional to the magnitude of the variation over the flux surface of the toroidal rotation frequency (Eqs (13) and (24)), in particular to the magnitudes of the vertical asymmetries in the rotation speed and density. All authors developed the gyroviscous theory within the context of the full viscosity tensor, decomposing the latter into 'parallel'. 'perpendicular' and 'gyroviscous' components.

The mathematical form of the gyroviscous force given in Ref. [8] and by Eqs (13) and (24) has not been questioned. What has been questioned, in two papers by Connor et al. [27, 28], is the theoretical basis for the magnitude of the variation over the flux of the toroidal rotation frequency, $\partial\Omega_\phi/\partial\ell_p$ or $\partial\Omega_\phi/\partial\theta$, in particular the magnitudes of the vertical asymmetries in density and toroidal rotation velocity. Thus, *it is not a question of the gyroviscous theory per se, but a question of the theoretical basis for evaluating the magnitudes of the vertical asymmetries in density and rotation velocity that is at the heart of the controversy.* Connor et al. [28] agree that if $|\partial\Omega_\phi/\partial\theta| \simeq |\epsilon\Omega_\phi|$, as suggested for certain circumstances by Stacey and Sigmar [8], then the gyroviscous theory (i.e. Eq. (29)) predicts the magnitude of the momentum confinement time inferred from experiment. In fact, Connor et al. do not dispute Eq. (29) (suppressing the profile factors h and the mass ratio correction — fine points that they did not consider) when multiplicative factors $G \sim O(1)$ and $\tilde{\theta}$ are included in the denominator. Thus, the only disagreement of Conner et al. [28] with the gyroviscous theory of Stacey and Sigmar [8] and with the theory presented in this paper is in the evaluation of the factor $\tilde{\theta}$, which has the form

$$\tilde{\theta} \simeq \left(3 + \frac{n_c}{\epsilon}\right)\left(\frac{v_s}{\epsilon}\right) + \left(1 - \frac{v_c}{\epsilon}\right)\frac{n_s}{\epsilon} \tag{56}$$

in the large aspect ratio approximation when density and rotation velocity variations over the flux surface are assumed to be represented by sine (vertical asymmetries) and cosine (horizontal asymmetries) components.

Stacey et al. [13b] solved the fluid momentum and particle balance equations to obtain explicit expressions for the density asymmetries, n_s and n_c, and for the toroidal rotation velocity

$$v_{\phi j} = \frac{K_j(\psi)B_\phi}{n_j} - \frac{R}{n_j e_j}\left(p_j' + n_j e_j \Phi'\right) \tag{57}$$

where ψ is the flux surface co-ordinate, the prime indicates a ψ-derivative, and K_j is a surface function determined from the separate parallel momentum balances on each species in the plasma. Stacey et al. [13b] also solved for the potential asymmetries, so Eq. (57) provided an implicit solution also for the asymmetries in rotation speed. The solution of Stacey et al. [13b] used Hirshman's extended form [29] of the Braginskij [25] 'parallel' viscosity to include trapped particle effects, which form reduces identically to the Braginskij form for the collisional regime, *plus* a 'drag' representation of the 'gyroviscosity'. Stacey [30] subsequently demonstrated that the representations used in Ref. [13b] could be derived from the formal gyroviscous theory under the condition that $|\partial\Omega_\phi/\partial\theta| \simeq |\epsilon\Omega_\phi|$, which is equivalent

to $|\tilde{\theta}| \sim O(1)$. When calculations were then performed [13b] for ISX-B and PLT plasmas, it was found that $|n_c^I| \sim |n_s^I| \sim O(\epsilon \bar{n}_I)$ for collisional impurities rotating near their thermal velocities, $v_{\phi I} \sim v_{thI}$, but that $|n_c^i| \sim |n_s^i| \ll O(\epsilon \bar{n}_i)$ for collisionless, banana-plateau (B-P) main ions rotating at a fraction of their thermal velocity, $v_{\phi i} \sim v_{\phi I} \sim v_{thI} \sim \sqrt{m_i/m_I}\, v_{thi}$. Thus, for the impurities, the result of the calculation was consistent with the assumption that was (implicitly) made to reduce the gyroviscous force to the drag form. From these calculations it was inferred in this paper and elsewhere that $|\tilde{\theta}| \sim O(1)$ for collisional impurities rotating near their thermal speeds and that $|\tilde{\theta}| \ll O(1)$ for B-P main ions rotating at a fraction of their thermal speed.

In their original paper [27], Connor et al. started with the same fluid particle momentum balance equations as in Ref. [13b], obtained Eq. (57) as a formal solution, but then used gyroradius and collisionality ordering approximations to argue that the K_j vanished and that Φ' was a surface function, to lowest order, and that the leading order contribution to gyroviscosity from the K_j term was of second order in the gyroradius parameter ρ_j/a, which was too small to account for the measured results. Connor et al. [27] were not explicit about their collisionality assumptions in their original paper [27], but they did treat an ion-electron plasma and ordered out frictional terms. In arguing that $\beta_I \ll 1$ in their second paper [28], Connor et al. implicity excluded the 'strong impurity' regime shown by Hsu and Sigmar [31] to support $O(\epsilon \bar{n}_I)$ vertical asymmetries in impurity density, which asymmetries would lead to gyroviscous forces large enough to account for the measured momentum confinement times [30].

In attempting to explain why their results differed from those of Stacey and Sigmar [8], Connor et al. [27] incorrectly stated that Stacey and Sigmar 'simply replaced' the Braginskij viscous stress tensor by the drag term, thereby omitting 'parallel' viscosity. Connor et al. were apparently unaware of the solution by Stacey et al. [13b] for arbitrary collisionality described in the preceding paragraph, in which 'parallel' viscosity plus the drag representation of gyroviscosity were included. Thus, the main criticism of the original paper by Connor et al. [27] was incorrect.

Partly in response to the criticism of Connor et al. [27], Stacey [30] summarized the gyroviscous theory and the theoretical and experimental evidence in the literature supporting $|\partial\Omega_\phi/\partial\theta| \simeq |\epsilon\Omega_\phi|$ for collisional impurities rotating near their thermal speed; suggested that Connor et al. [27] may have used ordering approximations that were inappropriate for strongly rotating plasmas with collisional impurities, causing them to order out some important terms that were retained in the numerical solution of Stacey et al. [13b]; and summarized the comparisons of gyroviscous theory predictions with experiment.

In their reply [28], Connor et al. (i) replace their initial criticism of omission of 'parallel' viscosity by a criticism of the form of the drag representation of gyroviscosity; (ii) argue from ordering assumptions that the Stacey [30] solution for K_j is 'unphysical' and hence that the calculation by Stacey et al. [13b] of asymmetries leading to $|\partial\Omega_\phi/\partial\theta| \sim |\epsilon\Omega_\phi|$ is 'flawed'; (iii) defend their alternative representation of the gyroviscous force against the criticism raised in Ref. [30]; (iv) admit that some of the theoretical literature cited in Ref. [30] supports $n_s \sim O(\epsilon \bar{n})$, while noting that some of it only supports $n_c \sim O(\epsilon \bar{n})$; (v) offer a general proof that impurities cannot give rise to $|\partial\Omega_\phi/\partial\theta| \sim |\epsilon\Omega_\phi|$; (vi) dismiss the suggestion that their ordering approximations could be inappropriate; (vii) state that they do not find the experimental evidence cited in Ref. [30] convincing; and (viii) dismiss the agreement between gyroviscous theory predictions and experiment as being fortuitous. Thus, in 1989, the year when Refs [28] and [30] were published, Connor et al. and Stacey agreed on the mathematical form for the gyroviscous force, but disagreed on the theoretical basis for estimating $\partial\Omega_\phi/\partial\theta$ and on the reason why they disagreed.

Connor et al. [28] believe that the drag representation of viscosity used by Stacey and Sigmar [13a] cannot be justified and that it led the latter authors to incorrectly calculate $|\partial\Omega_\phi/\partial\theta| \sim |\epsilon\Omega_\phi|$. Stacey [30] has given arguments justifying this representation. However, there has not been a first-principle neoclassical solution for Ω_ϕ with a rigorous representation of viscosity, so this theoretical question remains open.

While we believe that there is a neoclassical justification for $|\partial\Omega_\phi/\partial\theta| \sim |\epsilon\Omega_\phi|$, we note that if some anomalous mechanism produced this effect, the gyroviscous momentum transport rate would be sufficient to explain the experimental results.

Although Connor et al. [28] dismiss the suggestion [30] that ordering approximations could explain the disagreement, I maintain this opinion and believe that it is nicely illustrated by the recent work of Hsu and Sigmar [31]. These authors calculate the vertical asymmetry in impurity density in a strongly rotating plasma ($v_\phi \simeq v_{th}$) under two collisionality orderings, the usual neoclassical ordering and a 'strong impurity' ordering. In terms of the poloidal gyroradius parameter $\delta_{pj} = \rho_{pj}/L$, the self-collision frequency ν_{jj}, and the

transit frequency $\omega_{tj} = v_{thj}/L$, the usual neoclassical ordering is $\nu_{jj}/\omega_{tj} \simeq Z_j^{-2}$. For this ordering, Hsu and Sigmar find $O(\epsilon\delta_{pI}\bar{n}_I)$ vertical asymmetries in impurity density, which would lead to small gyroviscous forces that cannot explain the observed momentum confinement times, in agreement with the results of Connor et al. [27]. On the other hand, in the strong impurity ordering, $\nu_{jj}/\omega_{tj} \simeq \delta_{pj}^{-1}Z_j^{-2}$, Hsu and Sigmar find $O(\epsilon\bar{n}_I)$ vertical asymmetries in impurity density, which would lead to gyroviscous forces capable of explaining the observed momentum confinement times, in agreement with the results of Stacey et al. [8, 13b]. The sensitivity of the gyroviscous force to collisionality had previously been pointed out by Neeley [32], who found similar results.

The result of Hsu and Sigmar [31] bears strongly on the ordering approximation made by Connor et al. [28] in arguing that the results of Stacey et al. [13b] are a consequence of their drag representation and in defending their alternative representation against criticism by Stacey [30]. Connor et al. base their argument upon the assertion that the parameter

$$\beta_I \equiv \frac{\nu_{dI}}{\nu_{Ii}} = \frac{T/(2R^2ZeB)}{\nu_{Ii}} = \alpha\frac{\omega_{tI}}{\nu_{II}}\delta_{pI} \ll 1$$

While this assertion is true in the usual neoclassical ordering of Hsu and Sigmar, it is not in their 'strong impurity' ordering, where

$$\beta_I = \alpha\left(\delta_{pI}\frac{m_I}{m_i}\right)^2 \sim O(1)$$

for $\alpha \equiv n_I Z^2/n_i \sim O(1)$. Thus, the arguments which Connor et al. [28] present to support their contention that the solution of Stacey et al. [13b] for K_j is 'unphysical' and that the numerical result (no ordering approximations) that $|\partial\Omega_\phi/\partial\theta| \simeq |\epsilon\Omega_\phi|$ is 'flawed' are themselves invalid in the strong impurity limit of Hsu and Sigmar.

Numerical evaluation confirms that $\beta_I \sim O(1)$ for many current tokamaks, including JET.

The argument made by Connor et al. [28] that purports to demonstrate generally that $|\partial\Omega_\phi/\partial\theta| \ll |\epsilon\Omega_\phi|$ would also seem to be flawed by questionable ordering assumptions. The momentum input from the beam is implicitly ordered out at the outset; the frictional term, which Hsu and Sigmar [31] show to be important in the strong impurity ordering, is ordered out; and the surface function K is assumed to be small, presumably on the basis of their above discussed argument that was shown to be invalid in the strong impurity ordering.

Thus, I believe that Connor et al. [27, 28] have taken one set of ordering arguments (some of which are implicitly assumed) and worked through the consequences. I do not question the validity of their conclusions, for the plasma conditions defined by their implicit and explicit ordering assumptions, but I do question the universality of their results and in particular their applicability to present tokamak experiments. More to the point, Stacey et al. [13b] solved the rotation problem numerically, for the ISX-B and PLT plasma conditions, without making gyroradius or collisionality ordering approximations, and found results that are quite different from those of Connor et al. [27]. The latest explanation of Connor et al. [28] for the disagreement was shown above to be dependent upon ordering approximations which are of questionable applicability for collisional impurities in present-day, strongly rotating plasmas.

Although the need for a new set of ordering arguments for strongly rotating plasmas has been known for some time [33, 34], a consistent set of ordering arguments appropriate to present NBI plasmas, in which collisional impurities are rotating near their thermal velocity ($v_{\phi I} \simeq v_{thI}$) and B-P main ions are rotating at a fraction of their thermal velocity ($v_{\phi i} \simeq v_{\phi I} \simeq v_{thI} \simeq \sqrt{m_i/m_I}\, v_{thi}$), has not yet been developed. Hinton and Wong [35, 36] have recently made a major contribution by developing a consistent gyroradius ordering hierarchy for collisionless, B-P ions rotating near their thermal velocities ($v_{\phi j} \simeq v_{thj}$). While their treatment establishes a mathematical framework, it does not correspond to the physical situation in present tokamaks, either for the main ions, which are rotating at a fraction of their thermal velocity rather than near their thermal velocity, or for the impurity ions, which are collisional rather than B-P ions. In effect, the Hinton-Wong electric field ordering is too strong for the main ions, and their collisionality ordering is too weak for the impurity ions.

Hinton and Wong find that, for the case of B-P ions rotating near their thermal velocity, the gyroviscous momentum transport rate is too small to account for the experimental observations. This result is consistent with the result of Connor et al. [27]. However, it is also consistent with the result of Stacey et al., who find that the vertical asymmetries for B-P main ions are very small [13b] and, hence, the gyroviscous force is very small [8]. Hinton and Wong do not consider the case of collisional impurity ions rotating near their thermal velocity, which is the case for which Stacey et al. [13b, 8] and Hsu and Sigmar [31] would predict that it would lead to $O(\epsilon\bar{n}_z)$ vertical asymmetries in impurity density and thus to gyroviscous forces that

are large enough to account for the experimental observations.

It is worth noting that Hinton and Wong [35, 36] do find that gyroviscosity produces momentum transport, which confirms the similar finding by Braginskij [25], Kaufman [26], Stacey and Sigmar [8] and Hogan [37].

Thus, while there is an unresolved controversy regarding the magnitude of the poloidal asymmetry in rotation frequency that should be used to evaluate the gyroviscous force in Eqs (13) and (24), the magnitude assumed in this paper, namely $|\partial\Omega_\phi/\partial\theta| \simeq |\epsilon\Omega_\phi|$, is theoretically defensible, as discussed above and in Ref. [30]. Moreover, there is growing evidence that the resolution of the controversy may lie in the direction of a careful development of the ordering arguments appropriate to strongly rotating plasmas with collisional impurities and B–P main ions, and an examination of the transport consequences of such a development. This work is in progress.

8. SUMMARY AND CONCLUSIONS

The paper presents a formalism for constructing theoretical expressions for global momentum and energy confinement times and for the central rotation speed which are self-consistent with the common definitions of the corresponding experimental quantities. The formalism shows why the steady state momentum confinement time is shorter than the velocity decay time following termination of NBI. It has been demonstrated that in a strongly rotating plasma there is a viscous radial energy flux, associated with the work done by the rotating plasma against the viscous stress, in addition to the conductive and convective radial energy fluxes, and that this viscous energy flux degrades the energy confinement time. A computational model has been developed, on the basis of a gyroviscous model for the radial flux of angular momentum and for the radial viscous energy flux as well as on the basis of an approximate, single dominant impurity representation of the impurities that are responsible for these gyroviscous fluxes. A circular flux surface approximation, with non-circularity represented by an effective radius, has been used. Profile effects were explicitly included in the model.

The computational model has been applied to a substantial subset of the JET rotation database. Good agreement is obtained between the predicted and measured central rotation frequencies and momentum confinement times and the scaling of these quantities with certain parameters in the gyroviscous model, giving confidence that the model presented in this paper can provide guidance in interpreting rotation measurements and that the related predictions of the contribution of the viscous radial energy flux to the energy confinement time are reliable. The momentum confinement as well as the energy confinement were substantially better in H-mode discharges than in L-mode discharges. As much as a quarter of the total energy loss was predicted to be due to the viscous flux, in the most rapidly rotating discharges.

The computational model has also been applied to a TFTR beam power scan. Good agreement is obtained between the predicted and the measured central rotation velocities and momentum confinement times. Approximately one half of the measured degradation of energy confinement time with increasing beam power could be accounted for by the viscous radial energy flux.

The model presented in this paper predicts the magnitude of the momentum confinement time and the central rotation velocity over a wide range of JET discharges, which commends its utility in interpreting the rotational data that are being accumulated in JET and other tokamaks.

The fact that a significant fraction of the total energy loss in JET plasmas with strong rotation is due to the same mechanism that causes the momentum loss, combined with the fact that this mechanism vanishes when the plasma rotation vanishes, leads to two important conclusions. First, the energy confinement times with regard to convective and conductive transport losses (neoclassical and anomalous) are significantly larger than the measured energy confinement times in JET and in other strongly rotating tokamak plasmas. Second, for a given injected beam power into a tokamak, the energy confinement would be better for balanced injection than for unbalanced injection.

ACKNOWLEDGEMENTS

This work was performed while the author was in residence as a visiting scientist at the JET project. The author expresses his appreciation to the JET project for its hospitality (in particular to D.F. Düchs for hosting his visit), to his colleagues on the JET Team (in particular to M. von Hellermann, who was responsible for the rotation frequency measurements; to B. de Esch, whose similar calculations confirmed the SAS program used for this analysis; to L. Hopkins for assistance in setting up the SAS program), and to D. Stork and S.D. Scott for providing information about JET and TFTR, respectively.

REFERENCES

[1] SUCKEWER, S., EUBANK, H.P., GOLDSTON, R.J., et al., Phys. Rev. Lett. **43** (1979) 207; SUCKEWER, S., EUBANK, H.P., GOLDSTON, R.J., et al., Nucl. Fusion **21** (1981) 1301.

[2] BRAU, K., BITTER, M., GOLDSTON, R.J., et al., Nucl. Fusion **23** (1983) 1643.

[3] ISLER, R.C., WOOTTON, A.J., MURRAY, L.E., et al., Nucl. Fusion **26** (1986) 391.

[4] BURRELL, K.H., GROEBNER, R.J., St. JOHN, H., SERAYDARIAN, R.P., Nucl. Fusion **28** (1988) 3.

[5] BITTER, M., ARUNASALAM, V., BARNES, C., et al., Plasma Phys. Controll. Fusion **29** (1987) 1234.

[6] SCOTT, S.D., BITTER, M., HSUAN, H., et al., in Controlled Fusion and Plasma Physics (Proc. 14th Eur. Conf. Madrid, 1987), Vol. 11D, Part I, European Physical Society (1987) 65.

[7] STORK, D., BOILEAU, A., BOMBARDA, F., et al., ibid., p. 306.

[8] STACEY, W.M., SIGMAR, D.J., Phys. Fluids **28** (1985) 2800.

[9] STACEY, W.M., Fusion Plasma Analysis, Wiley-Interscience, New York (1981).

[10] SCOTT, S.D. (PPPL), personal communication, 1988.

[11] STORK, D. (JET), personal communication, 1988.

[12] STACEY, W.M., RYU, C.M., MALIK, M.A., Nucl. Fusion **26** (1986) 293.

[13a] STACEY, W.M., SIGMAR, D.J., Phys. Fluids **27** (1984) 2078.

[13b] STACEY, W.M., BAILEY, A.W., SIGMAR, D.J., SHAING, K.C., Nucl. Fusion **25** (1985) 463.

[14] HAZELTINE, R.D., WARE, A.A., Phys. Fluids **19** (1976) 1163.

[15] BARTIROMO, R., The JET High Resolution Bent Crystal Spectrometer, Rep. JET-P(88)11, JET Joint Undertaking, Abingdon, Oxfordshire (1988).

[16] BOILEAU, A., HELLERMANN, M. von, HORTON, L.D., SUMMERS, H.P., MORGAN, P.D., Nucl. Fusion **29** (1989) 1449.

[17] HAWKES, N.C., HELLERMANN, M. von, BOILEAU, A., et al., in Controlled Fusion and Plasma Heating (Proc. 15th Eur. Conf. Dubrovnik, 1988), Vol. 12B, Part III, European Physical Society (1988) 1061.

[18] STORK, D. (JET), personal communication, 1988.

[19] MURAKAMI, M., ARUNASALAM, V., BELL, J.D., et al., Plasma Phys. Controll. Fusion **28** (1986) 17.

[20] MURAKAMI, M., EDMONDS, P.H., HALLOCK, G.A., et al., in Plasma Physics and Controlled Nuclear Fusion Research 1984 (Proc. 10th Int. Conf. London, 1984), Vol. 1, IAEA, Vienna (1985) 87.

[21] SCOTT, S.D., FONCK, R.J., BITTER, M., et al., in Controlled Fusion and Plasma Heating (Proc. 15th Eur. Conf. Dubrovnik, 1988), Vol. 12B, Part I, European Physical Society (1988) 103.

[22] PAUTASSO, G., STACEY, W.M., SCOTT, S.D., et al., paper in preparation.

[23] PAUTASSO, G., SCOTT, S.D., HILL, K.W., et al., Bull. Am. Phys. Soc. **33** (1988) 1937.

[24] HAWRYLUK, R.J., ARUNASALAM, V., BELL, M.G., et al., in Plasma Physics and Controlled Nuclear Fusion Research 1986 (Proc. 11th Int. Conf. Kyoto, 1986), Vol. 1, IAEA, Vienna (1987) 51.

[25] BRAGINSKIJ, S.I., Rev. Plasma Phys. **1** (1965) 205.

[26] KAUFMAN, A., Phys. Fluids **3** (1960) 610.

[27] CONNOR, J.W., COWLEY, S.C., HASTIE, R.J., et al., Plasma Phys. Controll. Fusion **29** (1987) 919.

[28] CONNOR, J.W., COWLEY, S.C., HASTIE, R.J., Plasma Phys. Controll. Fusion **31** (1989) 1469.

[29] HIRSHMAN, S.P., Phys. Fluids **21** (1978) 224 and 1295.

[30] STACEY, W.M., Plasma Phys. Controll. Fusion **31** (1989) 1451.

[31] HSU, C.T., SIGMAR, D.J., Plasma Phys. Controll. Fusion **32** (1990) 499.

[32] NEELEY, G.W., Ion transport theory for a strongly rotating, beam-injected tokamak plasma, PhD Thesis, Georgia Institute of Technology (1987).

[33] HAZELTINE, R.D., Phys. Fluids **17** (1974) 961.

[34] BURRELL, K.H., OHKAWA, T., WONG, S.K., Phys. Rev. Lett. **47** (1981) 511.

[35] HINTON, F.L., WONG, S.K., Phys. Fluids **28** (1985) 3088.

[36] WONG, S.K., Phys. Fluids **30** (1987) 818.

[37] HOGAN, J.T., Phys. Fluids **27** (1984) 2308.

(Manuscript received 10 October 1988
Final manuscript received 17 July 1990)